A novel vibration-analysis based reliability quantification model for flexible coupling hub subjected to misalignment

Dr. Hussain VMS[1], Dr. Azhar Equbal[2*], Dr. Md. Israr Equbal[3], Prof. Zahid A Khan[2], Prof. Irfan Anjum Badruddin[4], Dr. Sarfaraz Kamangar[4]

[1]Department of Mechanical and Manufacturing Engineering, National Institute of Advanced and Manufacturing Technology, Hatia, Ranchi – 834003, India
Mb: 91-95642-50329

[2] Department of Mechanical Engineering, Jamia Millia Islamia, New Delhi – 110025, India
Tel: 91-11-26981259; Mb.: * - +917004564288

[3] Mechanical Engineering Section, University Boys Polytechnic, Aligarh Muslim University, Aligarh – 202001, U.P, India
Mb.: +919771838144

[4] Mechanical Engineering Department, College of Engineering, King Khalid University, Abha 61413, Asir, Saudi Arabia
Tel: +966-17-241-9521

Email ids: [1]vmshussain@niamt.ac.in, [2]azhr_eqbl06@jmi.ac.in*, [3]israr.ubp@amu.ac.in, [2]zahid_jmi@yahoo.com, [4]magami.irfan@gmail.com, [4]sarfaraz.kamangar@gmail.com

Abstract:

In this research paper, a novel real-time experimental reliability model is proposed, and system vibration signals are utilized to investigate and mitigate the impact of misalignment on components in rotor systems. To quantify reliability and comprehend the intricate relationship, we introduce modified design equations and employ a simulation-based methodology in the stress-strength interference approach. Additionally, we propose a framework for establishing safe and critical thresholds for parallel misalignment and rotational speed, aiming to meet specified reliability targets for the flexible coupling hub. The vibration analysis and subsequent illustration of the model in this research work shows that the reliability of the coupling is start deteriorating much before the first critical speed of the test-setup. Thus, this model proves effective in industrial rotor systems to manage misalignment levels among components designed for specific rotational speeds.

Keywords: Reliability; Rotor systems; Flexible-coupling; Misalignment; Vibration analysis; Stress-Strength interference.

1. Introduction

Misalignment, ranking second only to mass imbalance, poses a significant challenge in rotating systems, inducing vibrations that can lead to system failure or catastrophic incidents [1]. This prevalent issue stems from diverse factors, including manufacturing defects, assembly tolerance variations, thermal distortions, dynamic piping forces, and foundation instability. The resulting misalignments manifest in various forms such as parallel and angular misalignments, individually or in combination. To address rotor misalignment challenges in rotating machinery, couplings serve as essential components, facilitating power transmission between drive and driven shafts, without torsional slip [2]. The excess misalignment in the coupling induces the dynamic forces and moments resulting in vibrations, and it results in the failures of system components and failure of couplings itself [3, 4].

Couplings come in two primary types: rigid and flexible. While rigid couplings provide a direct and unyielding connection, flexible couplings are favored for their ability to accommodate misalignments. Within the realm of flexible couplings, the mechanically flexible coupling stands out for its prevalence in industries, particularly for handling misalignments within specific intensity thresholds [5, 6]. The detection and identification of faults, including misalignment, in rotating systems involves a thorough analysis of system signatures such as vibration, noise, wear debris, and thermal conditions [7, 8]. Comprehensive literature surveys [9-18] delve into various fault detection methods, while specific studies model forces generated by misalignments and analyze their effects on system vibration and patterns. These listed research literature and surveys also delve and illustrates model-based diagnostic techniques to identify the rotating system faults like misalignment, shaft-cracks etc.

The afore-listed literature and most other models available in the published research, proposed and discussed fault identification and diagnosis techniques in rotor systems under various operating conditions. In practical rotor systems, it is impossible to maintain a faultless system once operation begins. Under such conditions, ensuring the reliability of the entire system and its components is crucial for sustained optimal performance [19]. A review of the recent articles [20-23] on rotor system reliability reveals a significant number of publications in areas such as reliability analysis, uncertainties, and, more recently, the application of machine learning techniques in reliability engineering.

It has been found from the literature review that several models have also been proposed for uncertainty analysis and quantification [24-27]. These articles along with articles enumerated in last paragraph also list a substantial body of work on reliability models and analysis. However, the comprehensive survey of the published literature indicates that there is limited research connecting real-time fault intensity, machine signatures, and reliability quantification. It may also be noted that as far as authors' knowledge goes, the relationship between shaft misalignment faults, their effect on couplings, and reliability quantification have not yet been explored.

The reliability of the coupling *i.e.,* the coupling doing the intended function is crucial for reliability of the rotating system. Traditional design approaches for mechanical components often rely on safety margins, but Dasgupta [28] advocate for a more sophisticated method i.e. the Stress-Strength Interference (SSI) model. This model treats stress and characteristic strength as random variables, providing a more nuanced and probabilistic perspective on reliability. A brief and well-listed survey of research works on SSI models can be referred in for justifying the selection of SSI model for rotating system/component reliability for this research work [29, 30].

While theoretical models exist for reliability and mass imbalance [8, 29], a critical gap remains for a validated experimental model specifically addressing reliability and misalignment in rotating systems. This paper contributes to filling this gap by presenting an experimental model designed to quantify the reliability of a flexible coupling in real-time when misalignment occurs between drive and driven shafts. This research offers valuable insights that extend beyond theoretical frameworks, providing practical applications for enhancing reliability in industrial systems.

2. Proposed Model for Reliability Quantification

In this proposed model, we use the residual force generation methodology of model-based fault diagnosis [31, 32]. The residual force generation is utilized to estimate the amount of dynamic force exerted on the rotating system. The model discussed here utilizes the information of the dynamic-model of a rotating system [31, 33], it employs the amount of dynamic force difference between vibration signatures of faulty and non-faulty system, which is termed as residual force.

2.1 Generation of Residual Force

The vibrations produced in a healthy (faultless / non-faulty) rotating system is denoted by the linear equation of motion with displacement vector $x_o(t)$ at *N* degrees of freedom due to the functional/operational load of $F_o(t)$, expressed in (1). And the incidence of the fault (parallel-misalignment in this case) in the faultless system makes the dynamic machine-signature (*viz.* vibration) variations in the system. The fault occurrence causes additional load and effects the changes in vibration signature, and it is represented in equation (2).

$$\mathbf{M}\ddot{x}_0(t)+C\dot{x}_o(t)+Kx_o(t)=F_o(t) \tag{1}$$

$$\mathbf{M}\ddot{x}(t)+C\dot{x}(t)+Kx(t)=F_o(t)+\Delta F(t) \tag{2}$$

The intensity of the vibration variations in the system depends on the type of the fault, intensity of the fault and the location of fault occurrence. The vibration signature difference between the non-faulty system and faulty system will produce the residual-displacement (3), residual-velocities (4) and residual-accelerations (5).

$$\Delta x(t)=x(t)-x_o(t) \tag{3}$$

$$\Delta\dot{x}(t)=\dot{x}(t)-\dot{x}_o(t) \tag{4}$$

$$\Delta\ddot{x}(t)=\ddot{x}(t)-\ddot{x}_o(t) \tag{5}$$

The residual force ($\Delta F(t)$) equation is deduced by subtraction of equation (1) from equation (2), and represented in equation (6), while system-matrices (**M**, C, and K) remains constant. The reason for constant system-matrices in the residual force equation is due to the assumption of rotor system as linear, in this proposed model.

$$\mathbf{M}\Delta\ddot{x}(t)+C\Delta\dot{x}(t)+K\Delta x(t)=\Delta F(t) \tag{6}$$

This residual force ($\Delta F(t)$) deduced is utilized to calculate the magnitude of the fault and the place of its incidence. For calculating the near accurate residual force due to the presence of fault in the system, from the vibration signature, identical operating conditions, and vibration measurement condition to be met for both non-faulty and faulty rotating systems [31].

2.2 Procedure for Modal expansion

To determine the residual vector ($\Delta F(t)$) at all nodes of the system, it is necessary to have the residual vibration response (i.e., residual displacement, residual velocity, and residual acceleration) for all degrees of freedom (N) of the system. However, practical constraints often limit the measuring of vibration response only in a few degrees of freedom (n), where n is much smaller than N.

To determine the residual vibration across all degrees of freedom of the system from the measured residual vibration signature $\Delta x_n(t)$, the modal expansion technique is employed [34]. This technique is based on the principle of approximating the residual vibration as a linear combination of a limited number of eigenvectors ($\hat{\phi}$). The complete residual vector $\Delta x(t)$ can be approximated by employing a reduced modal matrix ($\hat{\phi}$), which comprises a set of mode shapes $\hat{X}_k$

$$\hat{\phi} = \left[\hat{X}_1, \hat{X}_2, \ldots \hat{X}_k\right] \tag{7}$$

The maximum count of mode shapes included within the reduced modal matrix $\hat{\phi}$. should logically not surpass the number of independently measured vibration responses contained in the $\Delta x_n(t)$, meaning that K should be less than or equal to n.

The measured residual vibration response $\Delta x_n(t)$, is connected to the full residual vector $\Delta x(t)$ through the utilization of the transformation matrix $\tilde{T}$. This transformation matrix $\tilde{T}$ relies on the modal matrix $\hat{\phi}$, and $\Delta x_n(t)$ is expressed as follows:

$$\Delta x(t) = \tilde{T}\, \Delta x_n(t) \tag{8}$$

In this proposed model, the System Equivalent Reduction Expansion Process (SEREP) is employed to expand the available measured data $\Delta x_n(t)$.he SEREP expansion methodology utilizes the SEREP transformation matrix to extend the few measured degrees of freedom to cover all degrees of the system [34]. The SEREP transformation matrix is expressed as:

$$\tilde{T} = [\phi]\left[\hat{\phi}\right]^g \tag{9}$$

Where $\left[\hat{\phi}\right]^g$ is given as,

$$\left[\hat{\phi}\right]^g = \left[\left[\hat{\phi}\right]^T \quad \left[\hat{\phi}\right]\right]^{-1}\left[\hat{\phi}\right]^T \tag{10}$$

Subsequently, the substitution of equation (8) in the equation (6) ultimately leads to the expression (11), which gives the estimated residual force at all degrees of freedom.

$$\mathbf{M}\tilde{\mathrm{T}}\Delta\ddot{\mathrm{x}}_{\mathrm{n}}(t)+\mathrm{C}\tilde{\mathrm{T}}\Delta\dot{\mathrm{x}}_{\mathrm{n}}(t)+\mathrm{K}\tilde{\mathrm{T}}\Delta\mathrm{x}_{\mathrm{n}}(t)=\Delta\mathrm{F}(t) \tag{11}$$

2.3 Effective Stress and Reliability Quantification

The additional dynamic load due to misalignment i.e., $\Delta\mathrm{F}(\mathrm{t})=F_{mis}$ must be arrived from the vector of equivalent load ($\Delta\mathrm{F}(t)$). Apart from the design stress (for which the system/component designed), additional dynamic load due to misalignment will subsequently add equivalent stress on the component/system, which will be computed from F_{mis}. In the design equations of the components (in this case flexible coupling hub), this additional stress is to be incorporated to get the effective stress. This process of obtaining the effective stress is shown in Figure 1 in the appendix I. The reliability quantification will be done using the effective stress.

<Insert Fig. 1>

The stress-strength interference (SSI) failure model explained in [28], is utilized in the reliability quantification model. The following SSI equation (12) computes the component/system reliability for all likely values of the component/system strength (S_{TH}) and all likely values of the stress (S_{ts}) exerted on the system due to faults.

$$R=\int_{-\infty}^{\infty} f_{S_{TH}}(S_{TH})\left[\int_{-\infty}^{S_{TH}} f_{S_{ts}}(S_{ts})\,\mathrm{d}S_{ts}\right]\mathrm{d}S_{TH} \tag{12}$$

3. Illustration for the proposed reliability quantification model

This illustration centers on the flexible coupling hub. The hollow shaft design equation for power transmission is employed for coupling hub design. Under ideal alignment, the coupling experiences only the shear stress. However, misalignment, specifically parallel misalignment (without axial compression), introduces torque and bending moment, resulting in both shear and normal stresses. To determine design stress considering both types of stress, Guest's, and Rankine's hollow shaft design equations (15, 16) are applied [35]. The recommended approach involves calculating design stress using both equations and selecting the higher value for optimal coupling hub design.

The shear stress and the normal stress in the coupling hub is to be computed using the following equation (13, 14).

$$\tau=\frac{16T}{\pi}\left(d_o \Big/ \left(d_o^4-d_i^4\right)\right) \tag{13}$$

$$\sigma = \frac{32M}{\pi}\left(d_o \middle/ \left(d_o^4 - d_i^4\right) \right) \tag{14}$$

The Guest’s theory of maximum shear stress (15) and Rankine’s theory of maximum normal stress is given below.

$$\tau_{design} = \frac{16}{\pi}\sqrt{M^2 + T^2}\left(d_o \middle/ \left(d_o^4 - d_i^4\right) \right) \tag{15}$$

$$\sigma_{design} = \frac{16}{\pi}\left(M + \sqrt{M^2 + T^2} \right)\left(d_o \middle/ \left(d_o^4 - d_i^4\right) \right) \tag{16}$$

The incorporation of bending moment (M_{mis}) and Torque (T_{mis}) developed due to the presence of parallel misalignment between the driven and drive shafts will give the effective shear stress equation (17) and effective principal stress equation (18).

$$\tau_{eff} = \frac{16}{\pi}\sqrt{\left(M + M_{mis}\right)^2 + \left(T + T_{mis}\right)^2}\left(d_o \middle/ \left(d_o^4 - d_i^4\right) \right) \tag{17}$$

$$\sigma_{eff} = \frac{16}{\pi}\left(\left(M + M_{mis}\right) + \sqrt{\left(M + M_{mis}\right)^2 + \left(T + T_{mis}\right)^2} \right)\left(d_o \middle/ \left(d_o^4 - d_i^4\right) \right) \tag{18}$$

The parameters inherent in effective stress equations (17 and 18), including the inner and outer radii, length, and ultimate strength of the coupling hub material, exhibit a stochastic nature due to various manufacturing discrepancies, operational factors, and environmental irregularities. This stochastic behavior introduces complexity into reliability calculations, especially in the absence of a substantial amount of field test data, which is often impractical to obtain. Consequently, a simulation technique, involving the generation of random numbers, is employed to derive values for the random variables [36]. This enables the computation of the effective stress exerted on the coupling hub.

The generation of continuous random variables that align with their stochastic characteristics and calculating outcomes for each realization within equations (17, 18), the effective stress values assume a probabilistic nature. Similarly, the ultimate shear strength and ultimate normal strength for the shaft, contingent upon the specific material type and shape, are generated to align with their stochastic properties.

The previously mentioned SSI equation (12) for reliability computation undergoes modification and is expressed in (19) for the maximum shear stress model, while the maximum normal stress model is articulated in equation (20). This modification allows for a comprehensive evaluation of the coupling hub's performance under maximum shear and normal stress conditions, further enhancing the analytical framework.

$$R = \int_{-\infty}^{\infty} f_{\varsigma}(\varsigma) \left[\int_{-\infty}^{\varsigma} f_{\sigma_{eff}}(\sigma_{eff}) \mathrm{d}\sigma_{eff} \right] \mathrm{d}\varsigma \tag{19}$$

$$R = \int_{-\infty}^{\infty} f_{\mathrm{T}}(\mathrm{T}) \left[\int_{-\infty}^{\mathrm{T}} f_{\tau_{eff}}(\tau_{eff}) \mathrm{d}\tau_{eff} \right] \mathrm{dT} \tag{20}$$

In the following section, illustration of the experimental work in the test- bed is given to measure the resulting vibrations, for stress calculations.

3.1 Experimental work

The experimental acquisition of vibration response is conducted using a machine fault simulator (MFS) testbed, as illustrated in Figure 2a (schematic representation), Figure 2b (snapshot of the test-bed -MFS) and Figure 3 (FEM model) in appendix I.

<Insert Fig 2a & 2b>

<Insert Fig. 3>

This testbed is designed to introduce various types of faults for experimentation. The FEM model is segmented into nine nodes, each possessing four degrees of freedom, including two translational and two rotational motions as discussed in Sudhakar & Sekar [37]. Practical and cost constraints (discussed in section 2.2) dictate that vibration response is measured only at node 3 (i.e., at the bearing-1 holder).

For vibration data acquisition, four ICP ® accelerometers with BNC connectors (Brand: PCB Piezotronics Inc., US) are utilized, operating in the 0.3 – 10 KHz range and providing 100mV/G sensitivity.

A 4 Channel Portable USB DAQ (Brand: Spectra Quest Inc.; specification: 24 bits ADC, 51.2 K samples/sec, 20KHz analysis frequency range, high-speed tach) data acquisition system and OROS software are employed for data collection and analysis. The acquired signals are undergone digital integration to determine displacement and velocity amplitudes from recorded acceleration data. MATLAB is utilized for data plotting and to create custom code for further data analysis.

Vibration response is assessed under fault-free conditions and with parallel misalignment introduced, ranging from 0.254×10^{-3} m to 1.016×10^{-3} m at speeds ranging from 500 rpm to 800 rpm. The MFS's rotational speed is maintained below its first critical speed of 9000 rpm. Sample plots of vibration responses are depicted in Figure 4 and Figure 5 (representing a faultless scenario), as well as Figure 6 and Figure 7 (with the presence of a fault – parallel misalignment) in appendix I.

<Insert Fig. 4>

<Insert Fig. 5>

<Insert Fig. 6>

<Insert Fig. 7>

The residuals vector, encompassing acceleration ($\Delta\ddot{x}(t)$), velocity ($\Delta\dot{x}(t)$), and displacement ($\Delta x(t)$ calculated under fault-free and parallel misaligned conditions, is input into equation (11). This includes system matrices (M, C, and K) and the transformation matrix ($\tilde{T}$) to obtain the residual force vector ($\Delta F(t)=F_{mis}$) for all degrees of freedom. Assuming linearity in the system, there are no changes in the system matrices. The resultant residual forces computed at different nodes of the testbed are illustrated in Figure 8 in appendix I.

3.2 Quantification of Reliability

The residual force values resulting from parallel misalignment are used to calculate additional bending moments and torques in the coupling hub, as detailed in sub-section 2.3 and as given in equations (13-18). These, along with other parameters, are employed into equations (17, 18) to derive effective stress values. In this illustration, after 300,000 simulation cycles, resulting values for random variables effective shear stress (τ_{eff}) and effective normal stress (σ_{eff}) are fitted into appropriate probability distributions. A similar approach is taken for getting the ultimate strength distribution and its parameters. In this illustration the shear stress and ultimate shear strength are taken into consideration for calculating reliability.

Post-simulation, shear stress (τ_{eff}) and ultimate shear strength (T) values adhere to a standard normal distribution. Integrating density functions into Equation (18) yields the reliability expression (21). Substituting distribution parameters into equation (21) determines the coupling hub's reliability.

$$R = 1-\Phi(z) \tag{21}$$

where $$z=\frac{\left(\mu_{\mathrm{T}}-\mu_{\tau_{eff}}\right)}{\sqrt{(\tilde{n}_{\mathrm{T}})^2+(\tilde{n}_{\tau_{eff}})^2}} \tag{22}$$

5. Experimental Work Results

The experimental procedure involved iterative execution with incremental adjustments in both parallel misalignment and rotational speeds. Vibration plots (illustrated in Figures 4 to Figure 7 in appendix I) unequivocally depict an augmentation in the vibration amplitude of the 2x running speed component, attributable to the system misalignment [38]. Spikes in the 1x and 2x speed components in Figure 5 in appendix I (faultless condition plot) are ascribed to residual faults within the system.

Residual force plots for all nodes, presented in Figure 8 in appendix I, distinctly indicate misalignment at nodes 1 and 2, specifically at the flexible coupling. Comparative analysis of plots across incremental rotational speeds and parallel misalignment reveals an escalation in residual force at the coupling with increased rotational speed and misalignment.

<Insert Figure 8>

Results from simulation cycles and the corresponding reliability of the coupling hub under varying misalignment (mis) values and rotational speeds (rpm) are tabulated in Table 1 given in appendix II and graphically represented in Figure 9 in appendix I. Examination of experimental outcomes suggests that, within the test setup, parallel misalignment has a negligible impact on reliability in the speed range of $25Hz$ to $90Hz$. The reliability hovers around 0.999 for the specified parallel misalignment range $0.254\times10^{-3}m$ to $1.016\times10^{-3}m$ at the given rotational speeds, indicating the safety of this misalignment and speed range in the utilized testbed.

<Insert Figure 9>

However, a notable decrease in reliability is observed at 95 Hz for all parallel misalignments exceeding $0.254\times10^{-3}m$, as shown in the reliability plots in Figure 9 in appendix I. Despite the test bed's critical speed being $150Hz$, the decision was made to halt experiments at $95Hz$ to prevent permanent damage to the testbed, its sub-assemblies, and critical components.

In the context of the test-bed conditions, a coupling hub is deemed safe if its reliability equals or exceeds 0.999 for a specified level of parallel misalignment. Below this threshold, the coupling hub is considered critical, potentially leading to operational distress in the coupling assembly. Even if the sub-assembly (flexible coupling) operates in a distressed state within the rotating system, it may generate heightened damaging vibrations, noise, and other machine signatures, culminating in catastrophic incidents.

To ensure elevated reliability and safety at higher speeds, it is recommended to control misalignment through routine condition monitoring and preventive maintenance.

6. Conclusion

An increase in misalignment within rotating systems, especially at higher rotational speeds, results in the generation of additional dynamic forces. This can ultimately lead to failures and potentially catastrophic accidents. In the context of this research, a real-time reliability model has been introduced, utilizing the real-time vibration response, and exemplified with a specific case of coupling-hub. This model proves to be an effective tool for anticipating the operational reliability of rotor systems afflicted by parallel misalignment by measuring their vibration amplitudes. By specifying a desired reliability level, the model can be employed to establish safe operational speed ranges for both existing and newly developed rotating systems.

The model outlined in this research holds practical significance in fields such as aviation safety, power generation equipment, and has potential applications in surface transport and shipping, particularly in cases involving large couplings.

7. Limitations and Future scope

The model proposed in this research work has been developed, and the experimental work has been carried out with the consideration of a single fault in the system under laboratory conditions. This limitation was applied because the proposed model is novel which aims at assessing how reliability decreases with increasing fault intensity, utilizing the real-time vibration signature. However, in real-world rotor systems, multiple faults, with varying intensities, often arise as the system begins to operate. Over time, these faults can affect systems' reliability, making it crucial to consider their combined effect when quantifying reliability.

Future research may extend this work to investigate competing faults in rotor systems. Concurrently occurring faults, such as imbalance, misalignment, oil-wrl, rotor-stator rub, and cracks, can be analyzed using the model to assess their combined effect on the reliability. Additionally, future studies may also focus on developing real-time reliability quantification models based on other machine signatures, such as thermal and acoustic data from the system.

Nomenclature:

F_{mis}	:	Force due to misalignment
$\mathbf{M}$	:	Mass matrix
$\mathbf{C}$	:	Damping matrix

K	:	Stiffness matrix
$\ddot{x}_0(t)$	:	Acceleration vector of faultless rotor system
$\dot{x}_o(t)$	:	Velocity vector of faultless rotor system
$x_o(t)$	:	Displacement vector of faultless rotor system
$F_o(t)$	:	Force vector of faultless rotor system
$\ddot{x}(t)$	:	Acceleration vector of faulty rotor system
$\dot{x}(t)$	:	Velocity vector of faulty rotor system
$x(t)$	:	Displacement vector of faulty rotor system
$\Delta F(t)$	:	Equivalent load vector
n	:	Measurable degrees of freedom
N	:	Degrees of freedom
$\Delta x_n(t)$	:	Measured residual vector
$\tilde{T}$	:	Transformation matrix
$\Delta x(t)$	:	Residual displacement vector
$\Delta \dot{x}(t)$	:	Residual velocity vector
$\Delta \ddot{x}(t)$	:	Residual acceleration vector
$\hat{\phi}$	:	Reduced modal matrix
$\hat{X}_1, \hat{X}_2, \ldots \hat{X}_k$		Mode shapes
$\Delta q(t)$	:	Modal coordinate vector
R	:	Reliability
S_{ts}	:	Stress in the coupling-hub
S_{TH}	:	Strength of the coupling-hub
$f_{S_{ts}}(S_{ts})$	:	Probability density function of stress
$f_{S_{TH}}(S_{TH})$	:	Probability density function of strength
τ	:	Shear stress
τ_{max}	:	Maximum shear stress
τ_{mis}	:	Shear stress due to F_{mis}
τ_{design}	:	Design shear stress
M		Bending moment
T	:	Torque
d_o	:	Outer diameter of the coupling-hub
d_i	:	Inner diameter of the coupling-hub/shaft diameter
σ_{max}	:	Maximum bending stress
σ_{design}	:	Design normal stress
τ_{eff}	:	Effective shear stress
M_{mis}	:	Bending moment due to misalignment
T_{mis}	:	Torque due to misalignment

σ_{eff}	:	Effective bending stress
T	:	Ultimate shear strength
$f_{\varsigma}(\varsigma)$	:	Density function of ultimate normal strength
$f_{\mathrm{T}}(\mathrm{T})$	:	Density function of ultimate shear strength
$f_{\tau_{eff}}\left(\tau_{eff}\right)$	:	Density function of effective shear stress
$f_{\sigma_{eff}}\left(\sigma_{eff}\right)$	:	Density function of effective normal stress
$\Phi(z)$	:	Standard cumulative normal distribution function
μ_{T}	:	Mean of ultimate shear strength
$\tilde{n}_{\mathrm{T}}$	:	Standard distribution of ultimate shear strength
$\mu_{\tau_{eff}}$	:	Mean of effective shear strength
$\tilde{n}_{\tau_{eff}}$	:	Standard distribution of effective shear strength
$[\,]^{T}$	:	Transpose

Acknowledgment

The authors extend their appreciation to the Deanship of Research and Graduate Studies at King Khalid University for funding this work through Small Research Project under grant number RGP.1/210/45

References:

1. Desouki, M., Sassi, S., Renno, J. et al. "Dynamic response of a rotating assembly under the coupled effects of misalignment and imbalance", *Shock and Vibration*, **2020(1)**, 8819676 (2020). https://doi.org/10.1155/2020/8819676.
2. Haifei, W. and Gong, J. "Dynamic analysis of coupling misalignment and unbalance coupled faults", *Journal of low frequency noise vibration and active control*, **38** (2), 1-4 (2019). https://doi.org/10.1177/1461348418821582
3. Xiao, L., Xu, Y., Sun, X., et al. "Experimental investigation on the effect of misalignment on the wear failure for spline couplings", *Engineering Failure Analysis,* **131**, p.105755 (2022). https://doi.org/10.1016/j.engfailanal.2021.105755

4. Krajňák, J., Homišin, J., Grega, R., et al. "The failures of flexible couplings due to self-heating by torsional vibrations–validation on the heat generation in pneumatic flexible tuner of torsional vibrations", *Engineering Failure Analysis*, **119**, p.104977 (2021). https://doi.org/10.1016/j.engfailanal.2020.104977
5. Gangsar, P. and Tiwari, R. "Signal based condition monitoring techniques for fault detection and diagnosis of induction motors: A state-of-the-art review", *Mechanical systems and signal processing*, **144**, 106908 (2020). https://doi.org/10.1016/j.ymssp.2020.106908
6. Mancuso, J.R. *Couplings and Joints: design, selection & application*, CRC Press (1999). ISBN: 0-8247-9950-X
7. Hussain V. M. S. and Naikan V. N. A. "Vibration Response Based Reliability Modeling for Rotor Systems with Imbalance", *Intl J of Performability Engineering*, **12**(3), p.283 (2016). https://doi.org/10.23940/ijpe.16.3.p283.mag
8. Hussain V. M. S. and Naikan V. N. A. "Reliability modeling of rotary systems subjected to imbalance", *Intl J of Performability Engineering*, **9**(4), p.423 (2013). https://doi.org/10.23940/ijpe.13.4.p423.mag
9. Zhang, C., Cao, P., Zhu, R. et al. "Dynamic modeling and analysis of the spline joint-flexible coupling-rotor system with misalignment", *J of Sound and Vibration*, **554**, p.117696 (2023). https://doi.org/10.1016/j.jsv.2023.117696
10. Fahmi, A. T. W. K., Kashyzadeh, K. R., and Ghorbani, S. "A comprehensive review on mechanical failures cause vibration in the gas turbine of combined cycle power plants", *Engineering Failure Analysis*, **134,** p.106094 (2022). https://doi.org/10.1016/j.engfailanal.2022.106094
11. Rezazadeh, N., De Luca, A., and Perfetto, D. "Unbalanced, cracked, and misaligned rotating machines: A comparison between classification procedures throughout the steady-state operation", *Journal of the Brazilian Society of Mechanical Sciences and Engineering*, **44**(10), p.450 (2022). https://doi.org/10.1007/s40430-022-03750-1
12. Wang, F., Dai, P., Wang, J., et al. "Vibration responses of the bearing-rotor-gear system with the misaligned rotor", *Machines*, **10**(4), p.267 (2022). https://doi.org/10.3390/machines10040267
13. Kumar, P. and Tiwari, R. "A review: multiplicative faults and model-based condition monitoring strategies for fault diagnosis in rotary machines", *Journal of the Brazilian*

Society of Mechanical Sciences and Engineering, **45**(5), p.282 (2023). https://doi.org/10.1007/s40430-023-04203-z

14. Badihi, H., Zhang, Y., Jiang, B., et al. "A comprehensive review on signal-based and model-based condition monitoring of wind turbines: Fault diagnosis and lifetime prognosis", *Proceedings of the IEEE*, **110**(6), pp.754-806 (2022). https://doi.org/10.1109/JPROC.2022.3171691
15. Raghavedra, K., Madan, M., Sujata, M., et al. "Failure of flexible couplings in environmental control system (ECS) of an aircraft", *Engineering Failure Analysis*, **125**, p.105401 (2021). https://doi.org/10.1016/j.engfailanal.2021.105401
16. Bouchra A., Ali, E. and Hassan, G. "Experimental study on energy consumption in rotating machinery caused by misalignment", *SN Applied sciences*, **2**, pp 1-6 (2019). https://doi.org/10.1007/s42452-020-3043-2
17. Zerbst, U. and Klinger, C. "Material defects as cause for the fatigue failure of metallic components", *Intl J of Fatigue*, **127**, pp.312-323 (2019). https://doi.org/10.1016/j.ijfatigue.2019.06.024
18. Zerbst, U., Madia, M., Klinger, C., et al. "Defects as a root cause of fatigue failure of metallic components. I: Basic aspects", *Engineering Failure Analysis*, **97**, pp.777-792 (2019). https://doi.org/10.1016/j.engfailanal.2019.01.055
19. Luo, C., Shen, L. and Xu, A. "Modelling and estimation of system reliability under dynamic operating environments and lifetime ordering constraints", *Reliability Engineering & System Safety*, **218**, p.108136 (2022). https://doi.org/10.1016/j.ress.2021.108136
20. Li, X. Q., Song, L. K. and Bai, G. C. "Recent advances in reliability analysis of aeroengine rotor system: a review", *Intl J of Structural Integrity*, **13**(1), pp.1-29 (2022). https://doi.org/10.1108/IJSI-10-2021-0111
21. Wang, M., Wang, C., Hnydiuk-Stefan, A., et al. "Recent progress on reliability analysis of offshore wind turbine support structures considering digital twin solutions", *Ocean Engineering*, **232**, p.109168 (2021). https://doi.org/10.1016/j.oceaneng.2021.109168
22. Payette, M. and Abdul-Nour, G. "Machine Learning Applications for Reliability Engineering: A Review", *Sustainability*, **15,** (7) p.6270 (2023). https://doi.org/10.3390/su15076270
23. Xu, Z. and Saleh, J. H. "Machine learning for reliability engineering and safety applications: Review of current status and future opportunities", *Reliability*

Engineering & System Safety, **211**, p.107530 (2021). https://doi.org/10.1016/j.ress.2021.107530

24. Fu, C., Sinou, J. J., Zhu, W., et al. "A state-of-the-art review on uncertainty analysis of rotor systems", *Mechanical Systems and Signal Processing*, **183**, p.109619 (2023). https://doi.org/10.1016/j.ymssp.2022.109619.
25. Zhang, J. "Modern Monte Carlo methods for efficient uncertainty quantification and propagation: A survey", *Wiley Interdisciplinary Reviews: Computational Statistics*, **13**(5), p. e1539 (2021). https://doi.org/10.1002/wics.1539
26. Zhao, Y., Zhu, Y. P., Lin, J., et al. "Fault features uncertainty quantification with parameters uncertainties of data-driven models and its application in rotor systems condition assessment", *IEEE Transactions on Instrumentation and Measurement,* **73**, pp.1-11 (2024). https://doi.org/10.1109/TIM.2023.3338665
27. Ma, X., Zhang, Z. and Hua, H. "Uncertainty quantization and reliability analysis for rotor/stator rub-impact using advanced Kriging surrogate model", *J of Sound and Vibration*, **525,** p.116800 (2022). https://doi.org/10.1016/j.jsv.2022.116800
28. Dasgupta, A. and Pecht, M. "Material Failure Mechanisms and Damage Models", *IEEE Transactions on Reliability*, **40**(5), pp.531-536 (1991). https://doi.org/10.1109/24.106769
29. Hussain, V.M.S. and Naikan, V.N.A. "Reliability and Imbalance Modeling of a Low-Pressure Turbine Rotor", *Intl J of Life Cycle Reliability and Safety Engineering*, **1** (2), pp.61-70 (2012). https://sresa.org.in/SRESAJOURNAL/2012b.pdf
30. Zhao, B., Xie, L., Zhang, Y., et al. (2021) "An improved dynamic load-strength interference model for the reliability analysis of aero-engine rotor blade system", *Institution of Mechanical Engineers Part - G: Journal of Aerospace Engineering*, **235**(11), pp.1355-1373 (2021). https://doi.org/10.1177/0954410020972898.
31. Jalan, A. K. and Mohanty, A. R. "Model based fault diagnosis of a rotor–bearing system for misalignment and unbalance under steady-state condition", *J of sound and vibration*, **327**(3-5), pp.604-622 (2009). https://doi.org/10.1016/j.jsv.2009.07.014
32. Ekanayake, T., Dewasurendra, D., Abeyratne, S., et al. "Model-based fault diagnosis and prognosis of dynamic systems: A review", *Procedia manufacturing*, **30**, pp.435-442 (2019) https://doi.org/10.1016/j.promfg.2019.02.060
33. Arun, K. J., Shital, P., and Gaurav, M. "A review on fault diagnosis of misaligned rotor systems", Intl J of Performability Engineering, **16**(4), p.499 (2020). https://doi.org/10.23940/ijpe.20.04.p1.499509

34. Avitabile, P. and Pingle, P. “Prediction of full field dynamic strain from limited sets of measured data”, *Shock and vibration,* **19**(5), pp.765-785 (2012). https://doi.org/10.1007/978-1-4419-9834-7_79
35. Kurmi, R.S. and Gupta J. *A Text Book on Machine Design*, Eurasia publishing House Lt., New Delhi (2020). ISBN-13. 978-8121925372
36. Wisudawan, A., Prastianto, R. W., Hadiwidodo, Y. S., et al. “A Critical Study on the Haldar and Mahadevan's Reliability Analysis”, *Procedia Earth and Planetary Science*, **14**, pp.47-56 (2015). https://doi.org/10.1016/j.proeps.2015.07.084
37. Sudhakar, G.N.D.S. and Sekhar, A.S. “Coupling misalignment in rotating machines: modeling, effects and monitoring”, *Noise and Vibration Worldwide*. **40** (1), pp.17-39 (2009). https://doi.org/10.1260/0957-4565.40.1.17
38. Jamshidi, H., Jafari, A.A. and Jamshidi, P. “Vibration behavior of misaligned rotor with the asymmetric shaft using Timoshenko beam theory”, *Scientia Iranica*, **30**(4), pp.1265-1278 (2023). https://doi.org/10.24200/sci.2022.57914.5473

List of Figures:

List of Tables:

Appendix-I

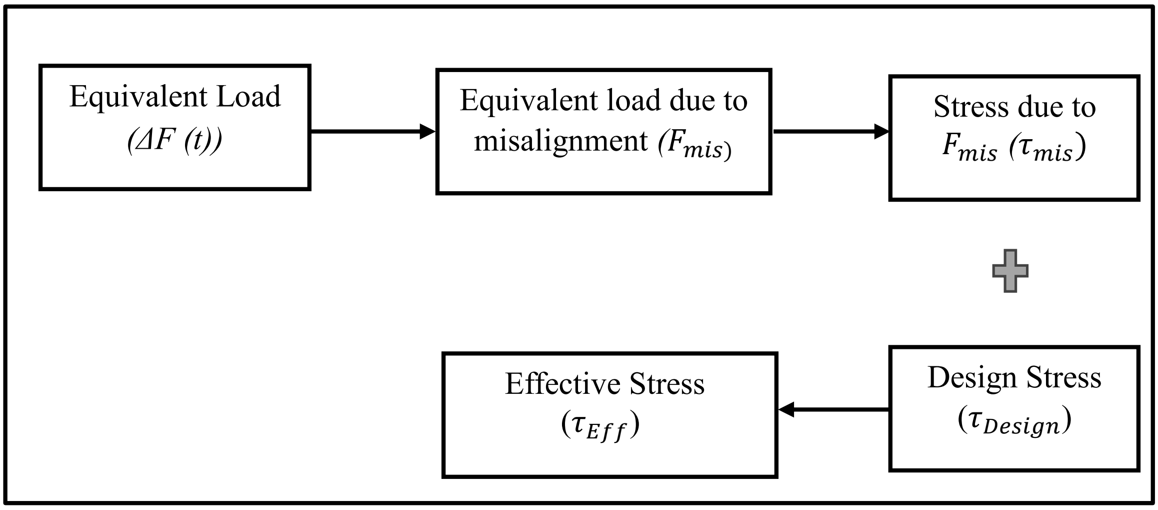

Figure 1: Computation of Effective stress

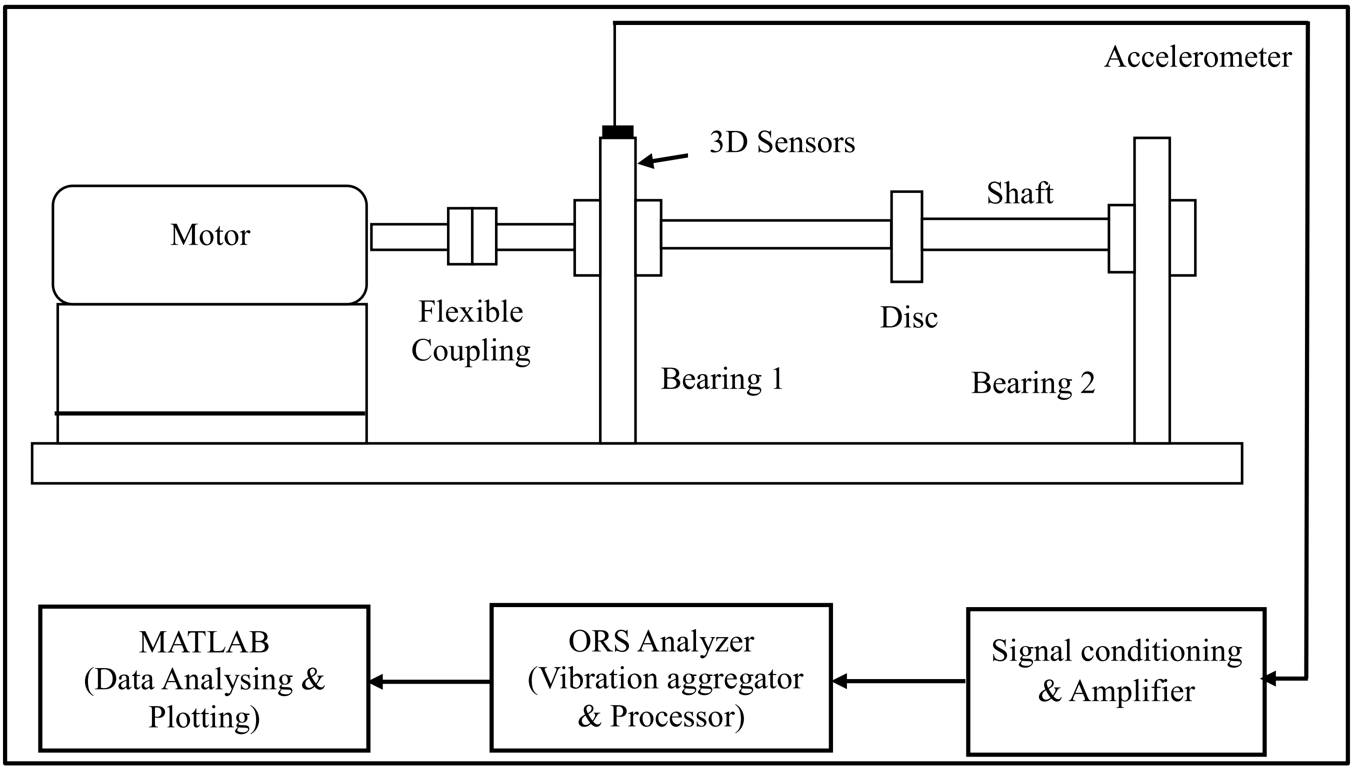

Figure 2a: Test-Bed schematic diagram

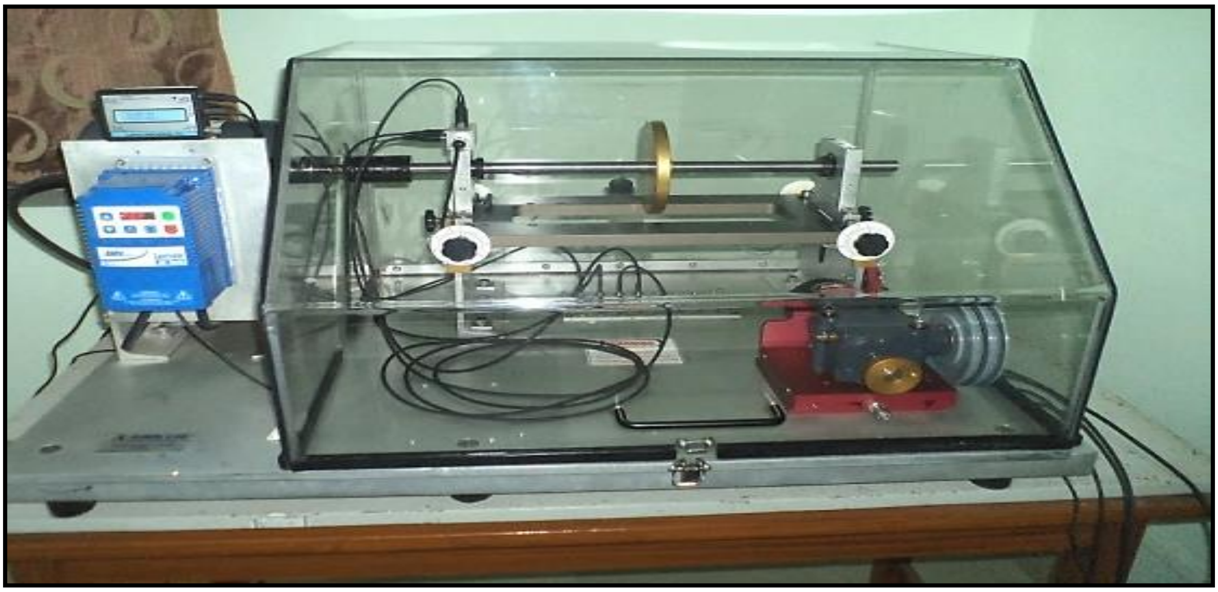

Figure 2b: Snapshot of Test-bed (Machine Fault Simulator – Brand: SpectraQuest)

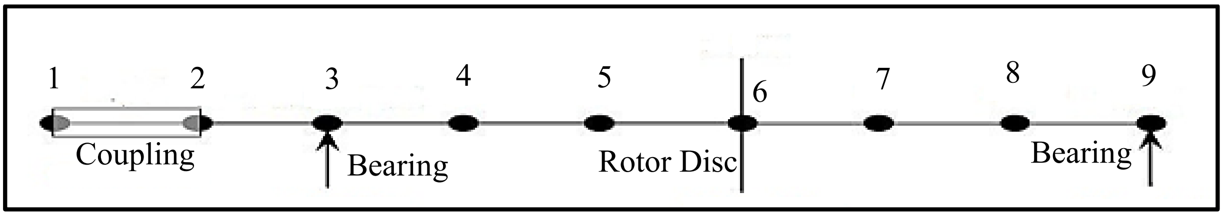

Figure 3: FEM model of Test-Bed

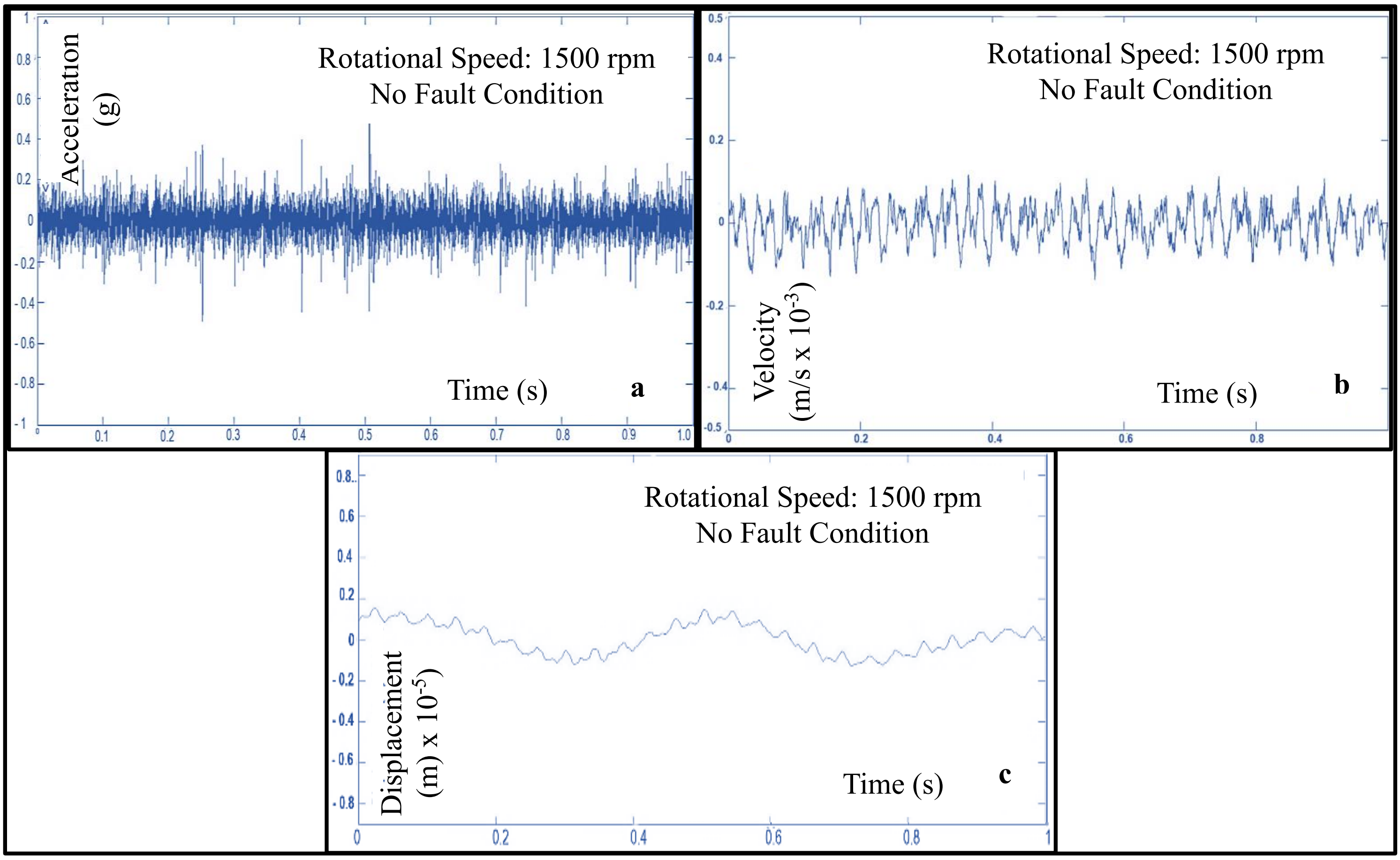

Fig. 4: Vibration response (at bearing–nearer to coupling) in x-direction without faults for 1500 rpm rotor speed. Time-domain plots of (a) acceleration (b) velocity and (c) displacement

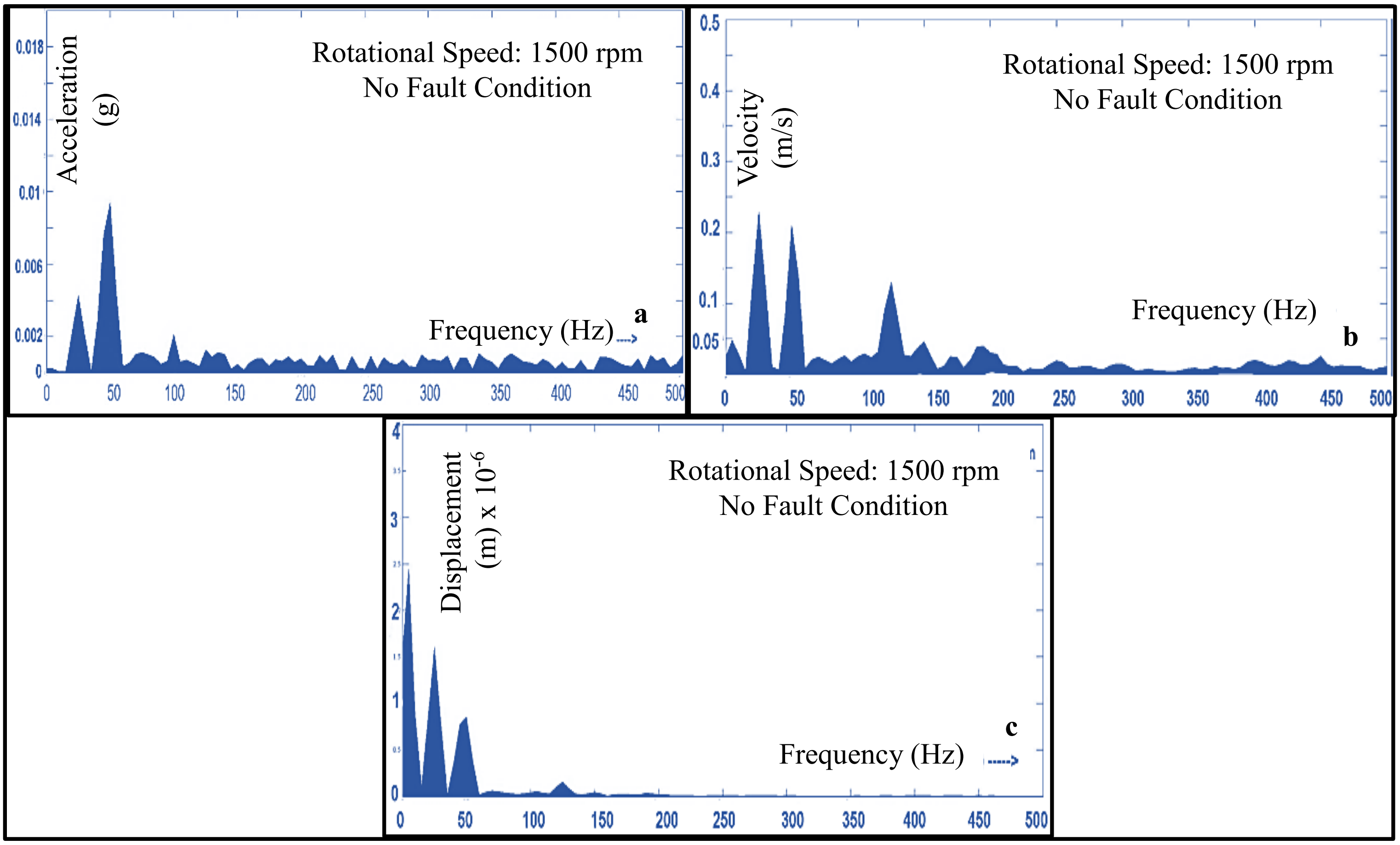

Fig. 5: Vibration response (at bearing–nearer to coupling) in x-direction without faults for 25 Hz rotor speed. Frequency-domain plots of (a) acceleration (b)velocity and (c). displacement

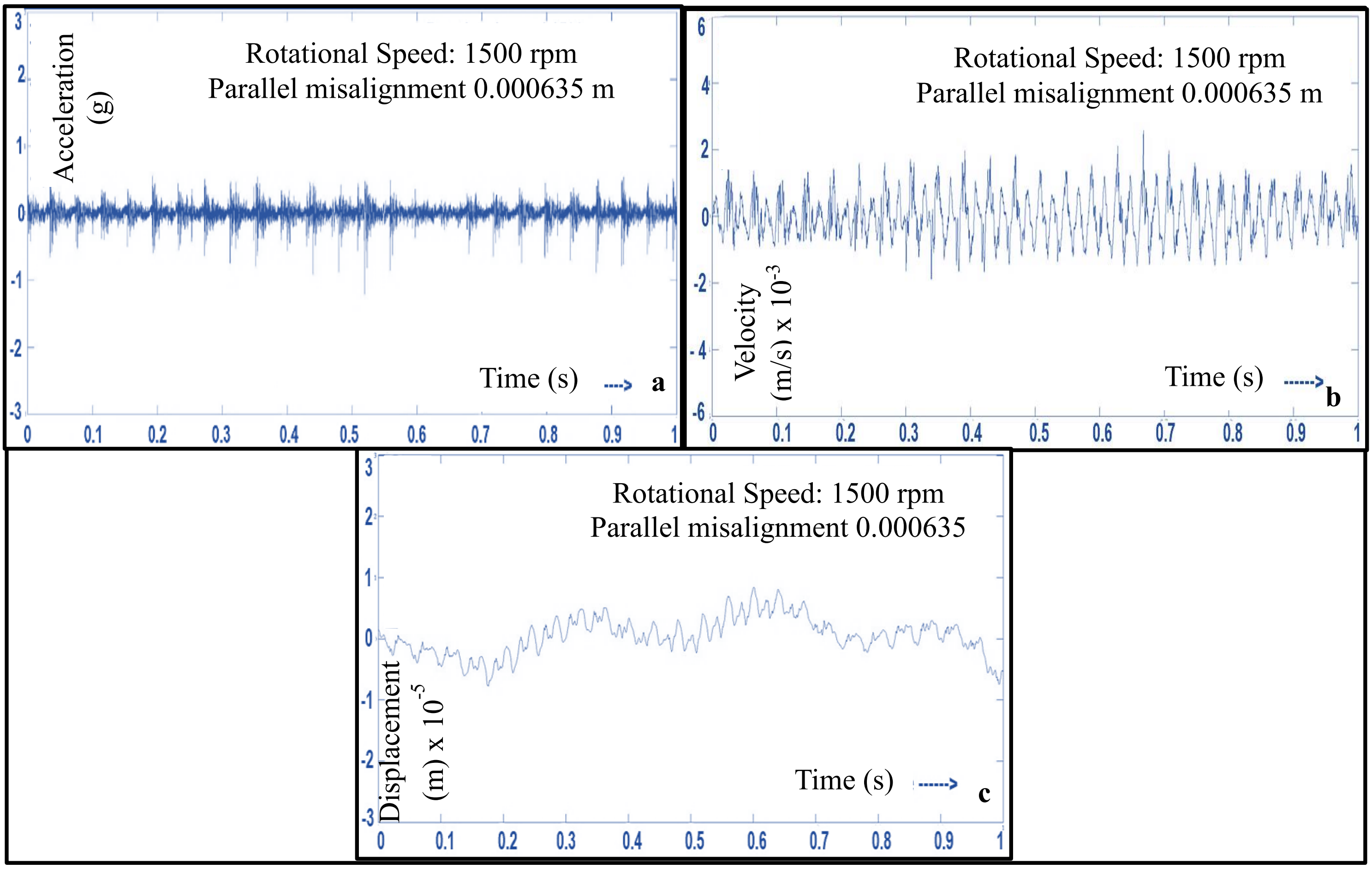

Fig. 6: Vibration response (at bearing–nearer to coupling) in x-direction with parallel misalignment (ΔX=0.000635 m, ΔY= NIL) for 1500 rpm rotor speed. Time-domain plots of (a) acceleration (b) velocity and (c) displacement

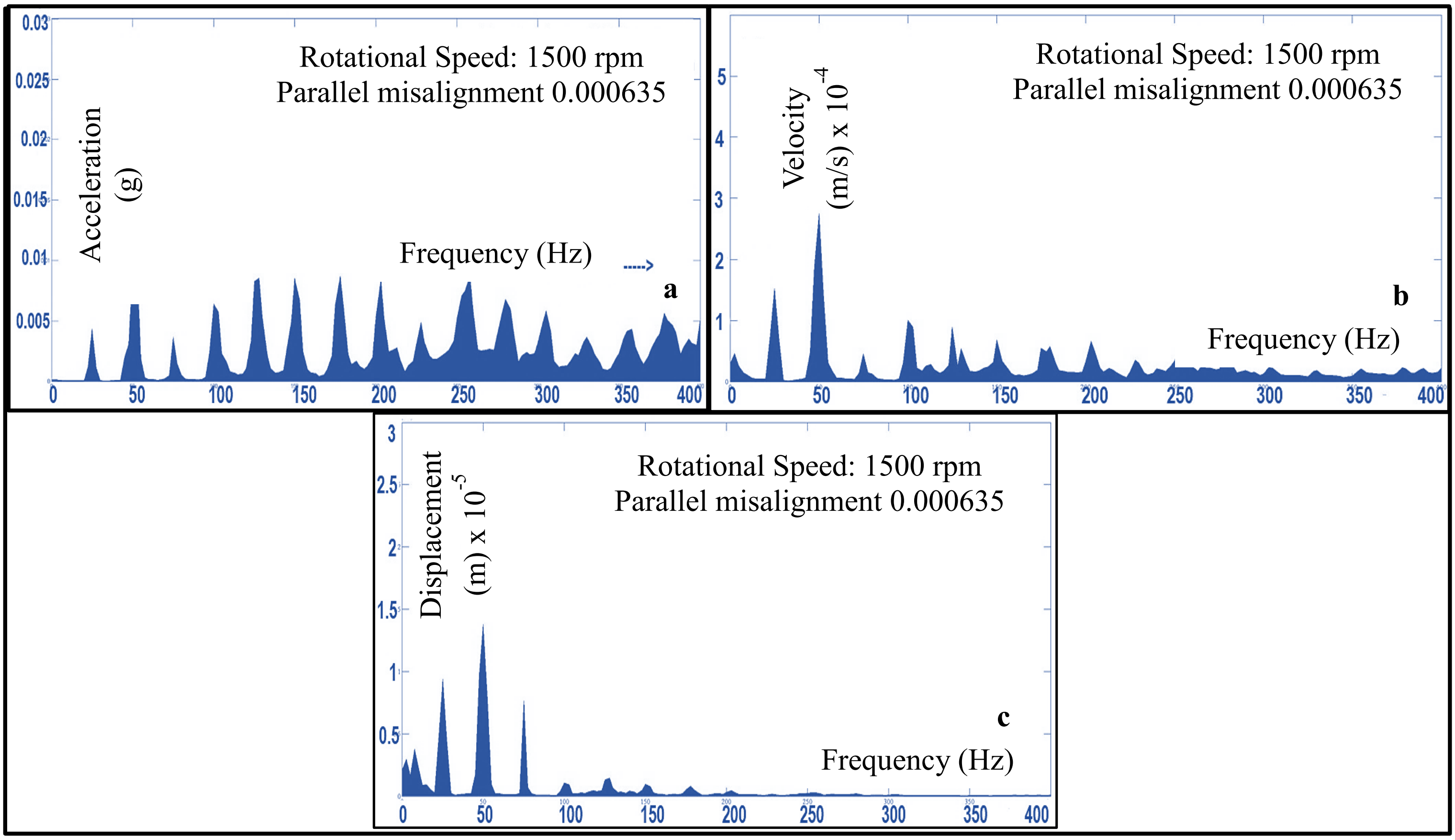

Fig. 7: Vibration response (at bearing–nearer to coupling) in x-direction with parallel misalignment (ΔX=0.000635 m, ΔY= NIL) for 1500 rpm rotor speed. Frequency-domain plots of (a) acceleration (b) velocity and (c) displacement

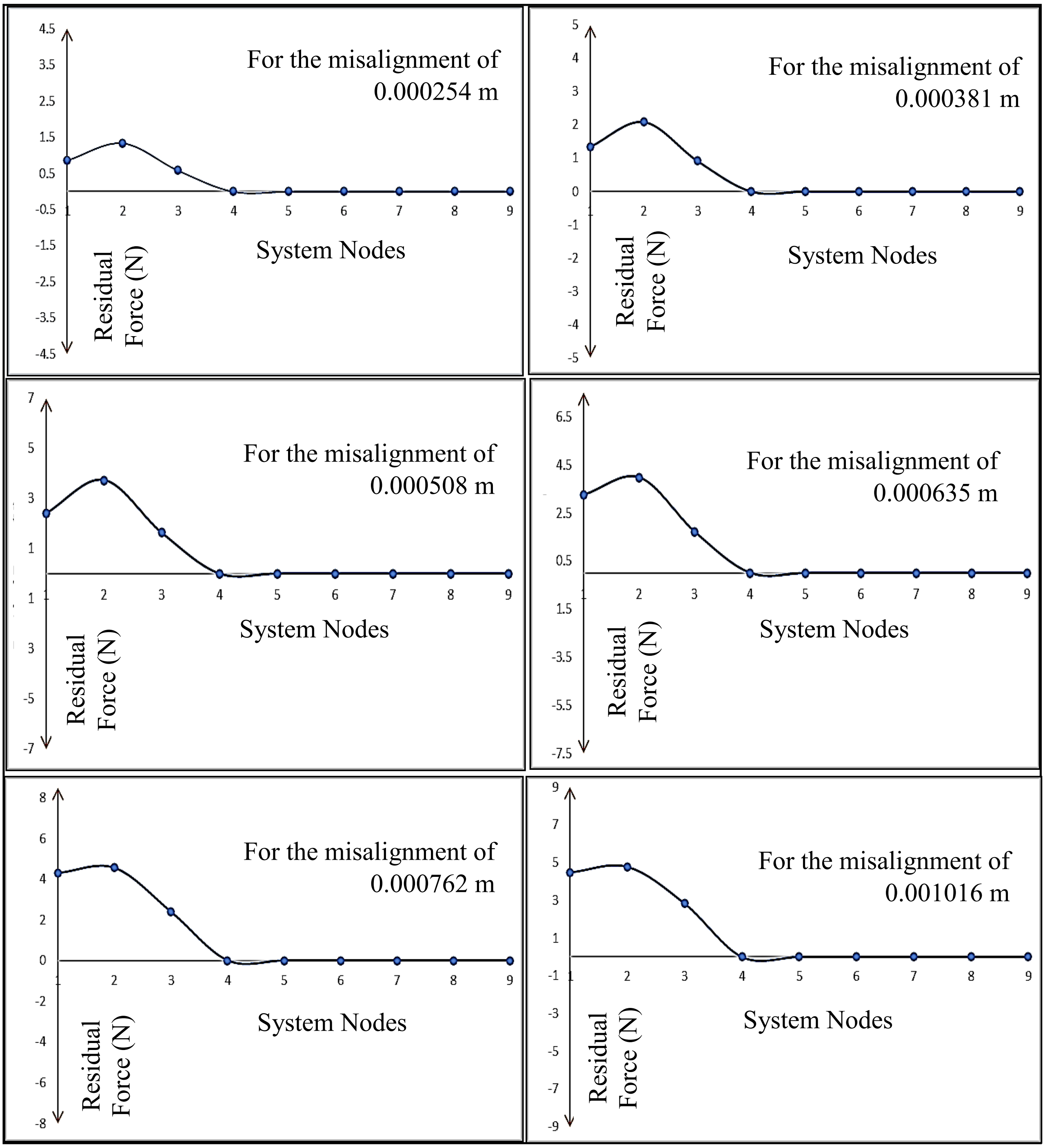

Fig. 8: Residual force due to misalignment at a rotational frequency of $45 Hz$ at different nodes of test-bed.

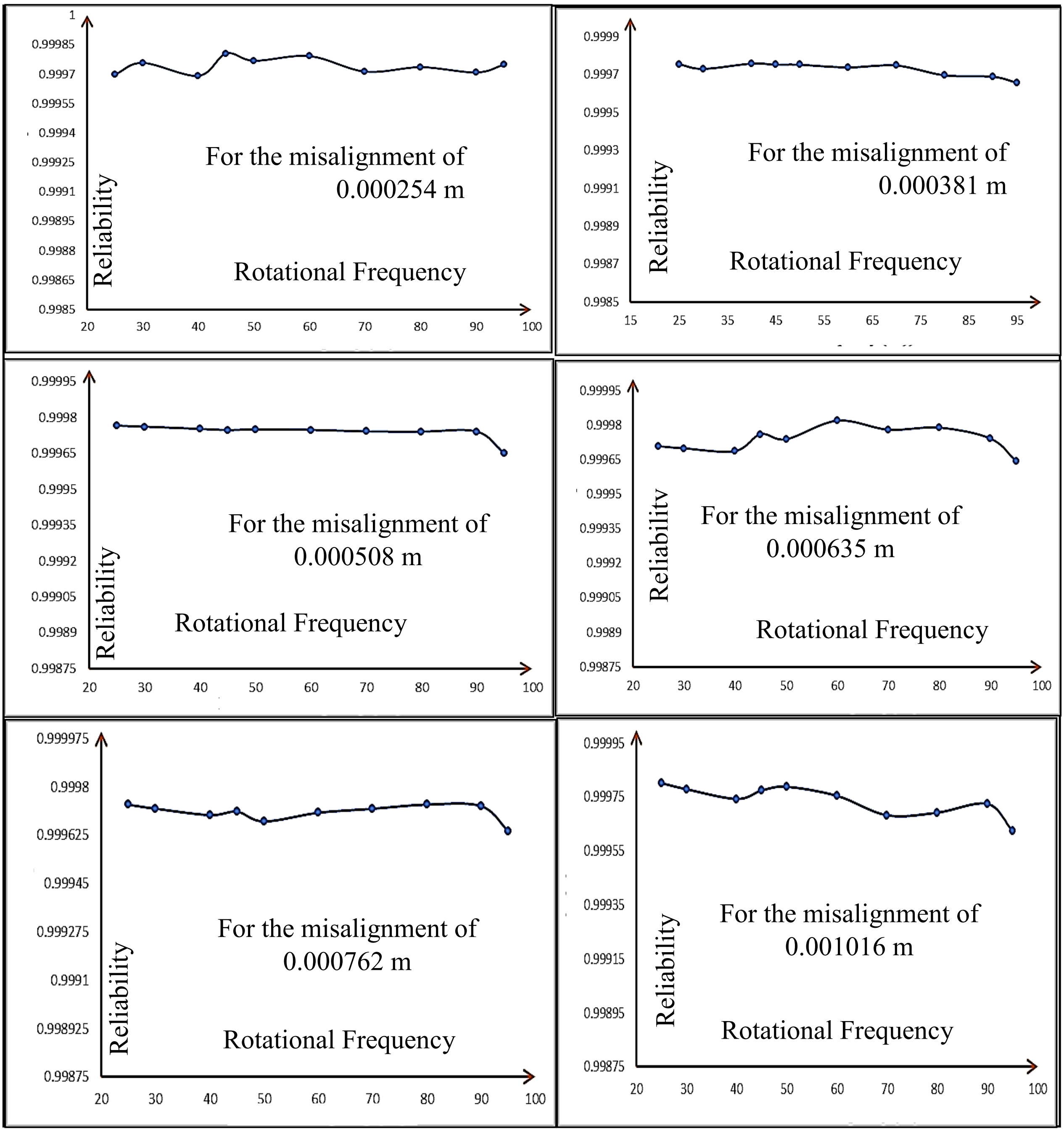

Fig. 9: Plots for reliability against rotational frequency (Hz) for various parallel misalignment measurement

Appendix II

Table 1: Quantified reliability for different misalignment settings and rotational speeds

Frequency ($\times 10^{-3}$ $\boldsymbol{m}$) → / Misalignment (Hz) ↓	0.254	0.381	0.508	0.635	0.762	1.016
25	0.999698	0.999756	0.999765	0.999708	0.999735	0.9998
30	0.999757	0.999732	0.999761	0.999698	0.999721	0.999778
40	0.999691	0.999759	0.999752	0.999687	0.999698	0.999742
45	0.999805	0.999753	0.999747	0.99976	0.99971	0.999773
50	0.999768	0.999753	0.999749	0.999738	0.999674	0.999787
60	0.999792	0.999739	0.999748	0.999819	0.999706	0.999753
70	0.999712	0.999749	0.999741	0.99978	0.99972	0.999682
80	0.999735	0.999698	0.99974	0.999789	0.999736	0.999692
90	0.999708	0.999691	0.999741	0.99974	0.99973	0.999724
95	0.999748	0.999659	0.99965	0.999642	0.999638	0.999624

Technical Biography of Authors:

Dr. Hussain VMS is an expert in reliability and systems safety engineering, holding a Ph.D. in reliability systems engineering, a master's in production engineering, and a bachelor's in mechanical engineering. His research and teaching focus on system reliability, safety engineering, and advanced manufacturing processes, contributing significantly to these critical areas. Dr. Hussain has published around 20 conference and peer-reviewed journal papers, with one earning the best research paper award at a conference hosted by Lawrence Technological University, Detroit, USA. As a committed mentor, he has supervised 24 master's dissertations and one Ph.D. thesis, fostering innovation and guiding future professionals in his field.

Dr. Azhar Equbal* is currently working in Mechanical engineering Department of Jamia Millia Islamia, New Delhi, India. He holds Ph.D. and Master's in Manufacturing engineering, and a Bachelor's in Mechanical engineering. His research and teaching focus on Basics of mechanical engineering, Manufacturing and Advanced manufacturing processes, Additive manufacturing, Operation research and, contributing significantly to these critical areas. Dr. Dr. Azhar Equbal has published more than 60 research papers in highly acclaimed peer-reviewed journal and around 20 conference papers.

Dr. Israr Equbal is currently working as an Associate Professor in Mechanical engineering Section, University Polytechnic, Aligarh Muslim University, Aligarh, India. He holds Ph.D. and Master's in Manufacturing engineering, and a Bachelor's in Mechanical engineering. His research and teaching focus on Manufacturing engineering, Advanced manufacturing processes, Metal forging, and Material science. His research findings contribute significantly to these critical areas. Dr. Israr Equbal has published around 40 research papers in highly acclaimed peer-reviewed journal and around 30 conference papers.

Dr. Zahid A Khan is currently working as Professor in the Mechanical engineering Department of Jamia Millia Islamia, New Delhi, India. His teaching and research areas include Friction Stir welding/Processing, Metal machining, Optimization of design and manufacturing, Multi criteria decision making (MCDM), ANN and Fuzzy Modelling and Ergonomics/Human Factors. He has more than 250 papers published in highly reputed and peer reviewed journals. He has supervised many Master's dissertations and Ph.D. theses, fostering innovation and guiding future professionals in his field.

Prof. Irfan Anjum Badruddin is a Professional at Mechanical Engineering Department of King Khalid University, Saudi Arabia. Prof. Irfan holds a PhD in Mechanical Engineering who works in interdisciplinary areas. He has many articles to his credit.

Dr. Sarfaraz Kamangar is currently working as Assistant professor at Mechanical Engineering, King Khalid University, Saudi Arabia. Dr. Sarfaraz completed his PhD from University Malaya. He works in the areas like Bio Mechanics, Fluid Dynamics, Materials and interdisciplinary etc. He has published more than 100 articles.